

Electronic Supplementary Information (ESI)

Compositional effect of Cr contamination susceptibility of $\text{La}_{9.83}\text{Si}_{6-x-y}\text{Al}_x\text{Fe}_y\text{O}_{26\pm\delta}$ apatite-type SOFC electrolytes in contact with CROFER 22 APU.

P.K.Pandis,^{a,b} E.Xenogiannopoulou,^c P.M.Sakkas,^b G.Sourkouni,^{d,e} C.Argirusis,^{b,e}
V.N.Stathopoulos,^{a,†}

^a Laboratory of Chemistry & Materials Technology, Department of Electrical Engineering, School of Technological Applications, Technological Educational Institute of Sterea Ellada, GR 34400, Psahna, Greece

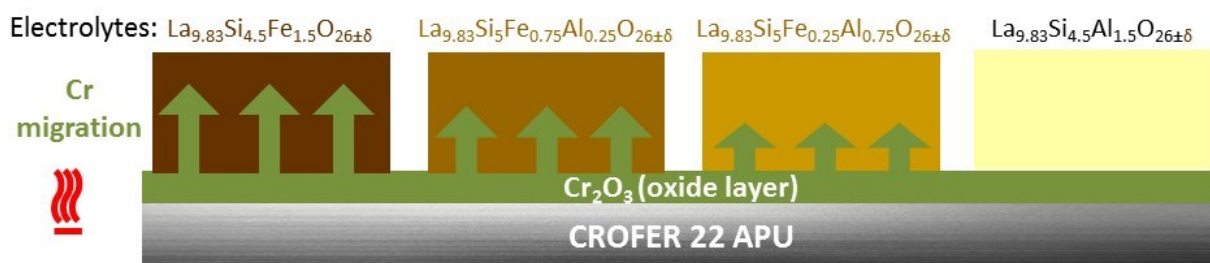
^b School of Chemical Engineering, National Technical University of Athens, 15780 Athens, Greece

^c Materials Industrial Research & Technology Center S.A., 72th klm of Athens-Lamia National Road, P.O.Box 18646, GR 34100 Chalkida, Greece

^d Institut für Energieforschung und Physikalische Technologien, Clausthal University of Technology, Robert-Koch-Str. 42, 38678 Clausthal Zellerfeld, Germany

^e Clausthaler Zentrum für Materialforschung (CZM), Agricola Str. 2, 38678, Clausthal Zellerfeld, Germany

Cross-section scheme of Cr migration in ATLS pellets in contact with CROFER 22 APU



[†]Corresponding author: vasta@teihal.gr; vasta@teiste.gr Laboratory of Chemistry & Materials Technology, Department of Electrical Engineering, School of Technological Applications, Technological Educational Institute of Sterea Ellada, GR 34400, Psahna, Greece

Contents

Particle Size Distribution Results.....	3
XRD Results.....	3
SEM-EDX Results.....	4
Impedance Measurements.....	6
References.....	6

Particle Size Distribution Results

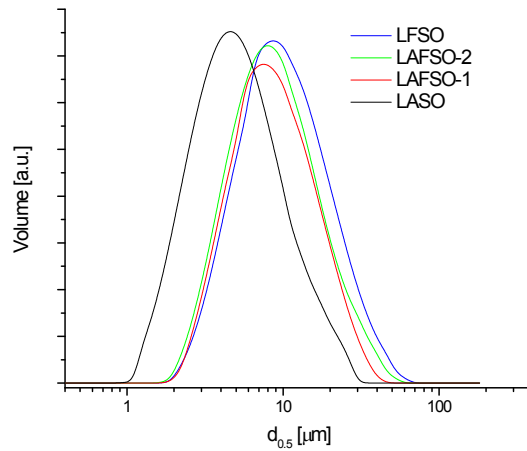


Figure 1S. Particle size distribution of ATLS powders before their sintering at 1500°C for 1h.

XRD Results

The formation of apatite phase was monitored by XRD. Typical XRD results for the apatite phase formation is shown in Fig.2S. Coexisting phases have been identified. Silicate apatite is formed and detected after the first firing step at 1400 °C. Further homogenization and thermal treatment eliminates secondary phases in the final materials.

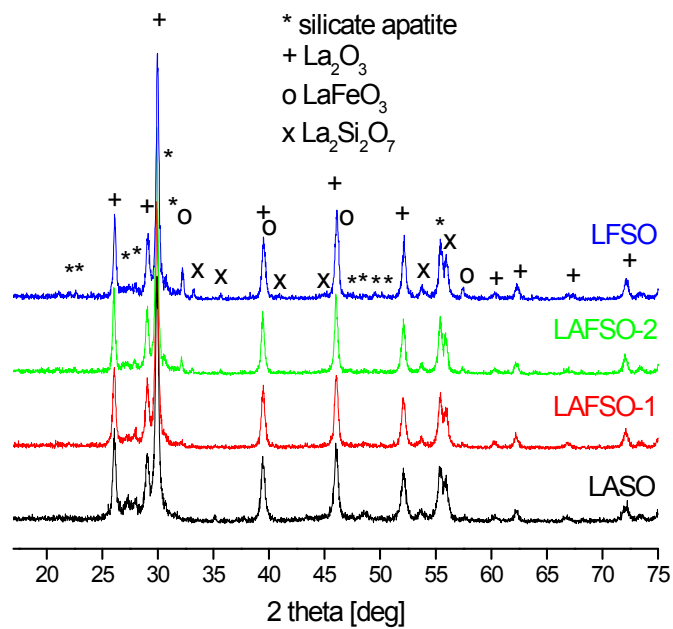


Figure 2S. Typical XRD profiles of all apatite samples precursors prior final firing at 1400 °C

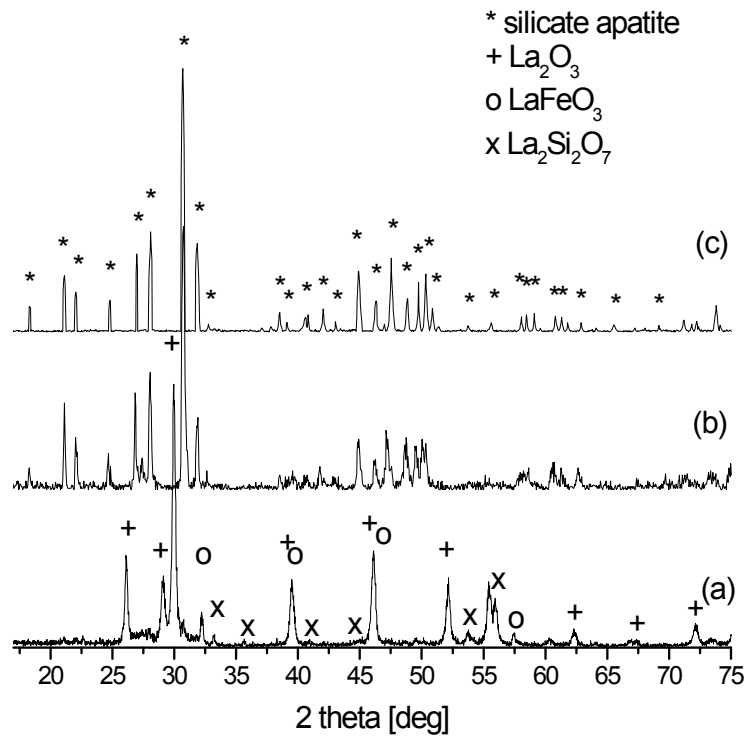


Figure 3S. XRD profiles of LFSO sample a) precursor fired at 1400 °C, b) after processing and final firing at 1400 °C and c) after sintering at 1500 °C

SEM-EDX Results

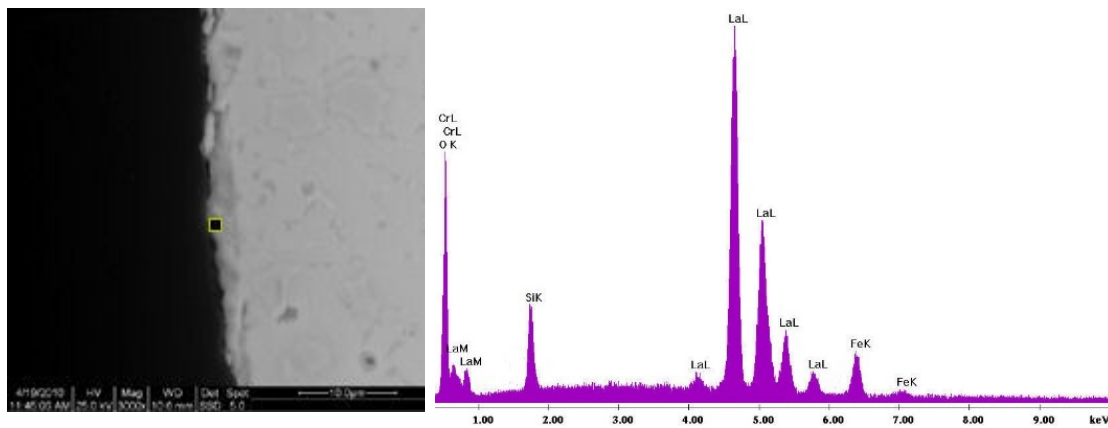


Figure 4S. SEM & EDX of LFSO in contact with CROFER22 APU after 1100°C/250h

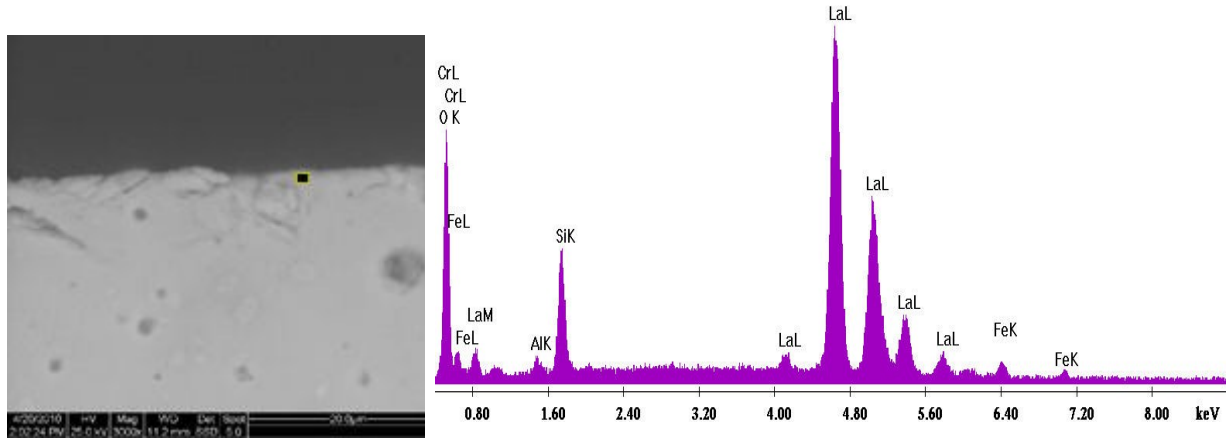


Figure 5S. SEM & EDS of LAFSO-2 in contact with CROFER22 APU after 1100°C/250h

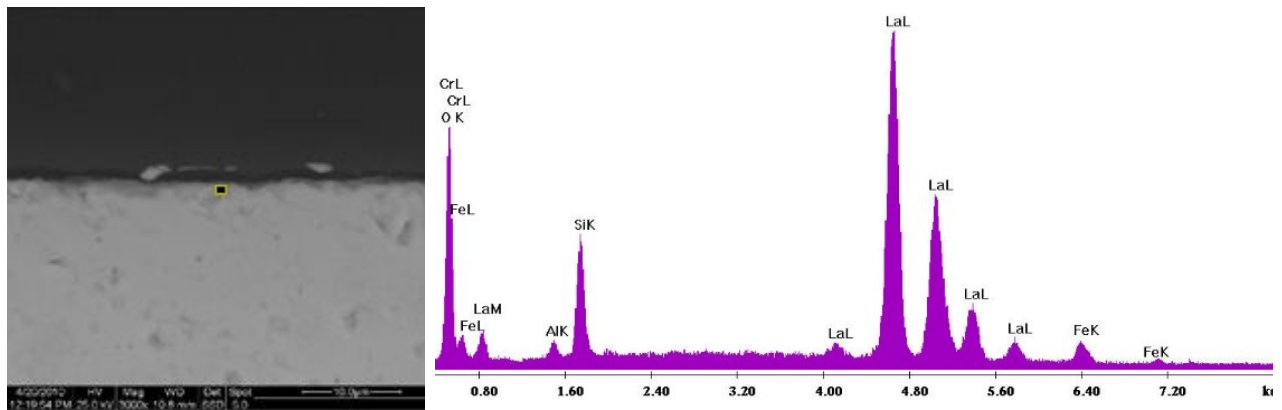


Figure 6S. SEM & EDS of LAFSO-1 in contact with CROFER22 APU after 1100°C/250h

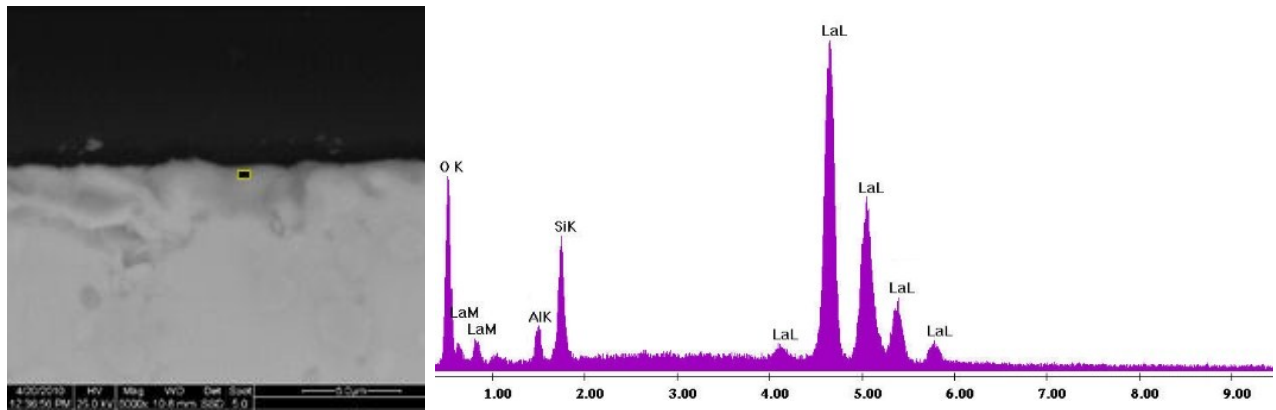


Figure 7S. SEM & EDS of LASO in contact with CROFER22 APU after 1100°C/250h

Table 1S. EDX results

Composition	Element Peak	wt %
LFSO	O (K)	20.56
	Cr (L)	0.89
LAFSO-2	O (K)	22.58
	Cr (L)	0.76
LAFSO-1	O (K)	21.05
	Cr (L)	0.56
LASO	O (K)	21.01
	Cr (L)	0.04

An indicative trend in Cr content could be elaborated using Cr (L) peak, showing Cr variation that follows the increasing Fe nominal composition in the apatite samples. Namely Cr (L) peak area was evaluated as negligible for LASO and largest for LFSO. This trend was similar in the ATLS samples for all thermal treatment protocols tested. Nevertheless, overlapping of Cr(L) and O (K) peaks was present in all cases. Cr(K) peak was not observed indicating in this case low confidence in the Cr content identification by EDX analysis.

Impedance Measurements

Pt porous electrodes were deposited on ATLS pellets by applying organometallic Pt-paste. Calcination was followed up to 850°C for 30 min with an intermediate step at 450°C for 30min. Pellets were clamped as reported in our earlier work [1] using Pt instead of Au. The impedance spectra were obtained in air from 800°C to 600°C applying a stimulus of 20mV within the frequency range of 1MHz to 10mHz. The materials treated at 1000°C/500h in contact with CROFER22 APU were used for impedance measurements.

The fitting profile used for the impedance spectra is represented in Figure 7S. Electrode resistance was negligible at higher temperatures.

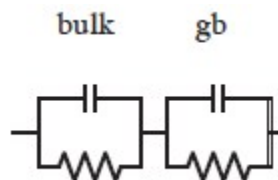


Figure 8S. Fitting profile used for the calculation of the conductivities.

References

1. H. Gasparyan, S. Neophytides, D. Niakolas, V. Stathopoulos, T. Kharlamova, V.Sadykov, O. Van der Biest, E. Jothinathan, E. Louradour, J.-P. Joulin, S. Bebelis, *Solid State Ionics*, 2011, **192**, 158.